



## Petrogenetic implications of granitoids from the Eqat area, South Eastern Desert, Egypt

Nahla A. Shallaly<sup>1</sup>, Mahmoud E. El-Mezayen<sup>2</sup>, Mohamed A. El-Sharkawi<sup>1</sup>, Mohamed I. El-Sibai<sup>2</sup>, and Ashraf Azab<sup>3</sup>



<sup>1</sup> Geology Department, Faculty of Science, Cairo University, Giza, Egypt

<sup>2</sup> Egyptian Mineral Resources Authority, Abbasyia, Egypt

<sup>3</sup> Nuclear Materials Authority, Cairo, Egypt

**T**HE EQAT area is located in the Southern Eastern Desert near Shalateen Town. It comprises a thrust-fold belt of an ophiolitic mélangé and an island arc metavolcano-sedimentary assemblage intruded by four magmatic bodies. Field relations and textural criteria indicate that these bodies belong to the syn-orogenic and post-orogenic granitoids widespread in the northern ANS. The syn-orogenic granitoids are exemplified by the Allaqi batholith to the west, which is composed of multiple coalesced plutons, and the Hoteib pluton to the north. Both which intrude the island arc assemblage and the ophiolitic mélangé are of diorite/Qz diorite to tonalite composition and a gneissose fabric parallel to the foliation of the country rock. The post-orogenic granitoids are represented by the elongated Heleikonti batholith to the east and the Eqat plutons in the center of the area. These granitoids are composed of tonalite, granodiorite, and monzogranite, with an overall undeformed magmatic fabric. Textural criteria indicate that both groups are affected by local mylonitization along the Eqat shear zone, i.e., this shear zone postdates the magmatic processes. The recorded shear sense indicators in both groups highlight the sinistral sense of shear of the Eqat shear zone, which formed at greenschist facies conditions. Geochemically, these rocks are I-type, calc-alkaline to slightly alkaline, and of volcanic arc to within plate affinity, which was emplaced along a 20-30km thick crust.

**Keywords:** Petrography, Geochemistry, Volcanic arc granites, Eqat shear zone.

### Introduction

As part of the Arabian Nubian Shield (ANS), 50% of the Egyptian Precambrian rocks are granitic in composition (e.g., Moghazi et al., 2004). Their predominance led several authors to propose different classification schemes (e.g., El Shazly, 1964; El Ramly, 1972; Akaad and Noweir, 1980; Hussein et al., 1982; Ries et al., 1983; El Gaby et al., 1984; Bendor, 1985; Hassan and Hashad, 1990). Generally, two magmatic episodes are recorded, the older (750- 610 Ma) and the younger (610- 580 Ma), which exhibit compositional, chemical, and tectonic variations (e.g., Farahat et al. 2007; Moussa et al. 2008; El-Bialy and Hassen, 2012; Azer 2013; Eliwa et al. 2014; Basta et al., 2017). This continuous array of magmatism played a significant role in the evolution of the Arabian Nubian Shield crust.

The Eqat (Egat) area was long known for its gold potentiality, including the historic gold mines of Umm Egat/ El Fawi (Klemm and Klemm, 2013). It

is located southwest of the Shalatin area, the Southern Eastern Desert between latitudes 22° 00'00"-22° 17'00" N and longitudes 34° 45'00"-35° 06'00" E. The region comprises a thrust-fold belt of an ophiolitic mélangé, part of the Allaqi-Heianai shear zone's northwestern termination of the Hamisana shear zone (Greiling et al., 2014). The mélangé consists of differently sized blocks of serpentinized ultramafic, metagabbros, amphibolites, sheeted dykes, and pillow basalts in a highly sheared pelitic to serpentineous matrix. This mélangé is in thrust contact with an island arc metavolcano-sedimentary sequence. This sequence comprises intermediate to acidic volcanic flows and pyroclastics with subordinate schistose metasediments. Both units are intruded by magmatic rocks and dykes (Nasr et al., 1998; Oweiss and Said, 2000; Salem, 2007; Zohier and Emam, 2012). Structurally, the area has experienced two deformational phases resulting in the development

\*Corresponding author e-mail: shallalynahla@cu.edu.eg

Received: 23/04/2025; Accepted: 24/05/2025

DOI: 10.21608/egjg.2025.372963.1110

©2025 National Information and Documentation Center (NIDOC)

of WNW-trending, followed by NW-to-NNW-trending, overturned folds, and their associated planar and linear fabrics. These compressional phases were followed by developing NNW-trending shear and mylonitic zones and conjugating NNW–SSE and WNW–ESE sinistral and dextral strike-slip faults (Zohier and Emam, 2012). The current study focuses on studying the petrographical and geochemical characteristics of Eqat granitoids to constrain their petrogenetic and geodynamic evolution.

### Materials and techniques

Thin and polished sections of 40 samples were made to study their petrographic characters. Nineteen representative samples covering the different granitic rocks and localities are carefully selected from the collected samples for chemical analyses. The analyses were conducted on fused and pressed powder pellets for major oxides and trace elements using X-ray fluorescence equipment PW 2404. Selected REE analyses for five samples were performed using a simultaneous inductive coupled Plasma Optical Emission Spectrometer (720 ICP-OES, Agilent Technologies). All techniques were conducted in the Central Laboratories of the Egyptian Mineral Resources Authority (EMRA), Dokki, Egypt.

### Results and Discussion

#### Geologic setting

Four magmatic bodies are exposed in the Eqat area, intruding into the ophiolitic mélangé and the island arc assemblage. The largest is the Allaqi batholith (Figs.1 & 2), extending to the west, southwest of the study area and Sudan. This low-to-medium relief and rounded batholith (350 km<sup>2</sup>) is traversed by the WNW-ESE Wadi Allaqi (Fig. 3A). It intrudes the island arc metavolcano-sedimentary belt with a gradational contact. The rocks of this batholith are of multiple coalesced plutons of light to dark grey, coarse to medium-grained gneissose felsic to intermediate composition, which exhibit different degrees of alteration and suffer ductile and brittle deformations. Ductile deformation is exemplified by its overall foliated and lineated fabric, whereas normal faults and conjugate joints demonstrate

brittle deformation; near the faults, the low-angle foliations become steep. Differently sized elongated black-to-gray xenoliths of the island arc metavolcanics are wrapped around by the foliation of these magmatic rocks. The 132km<sup>2</sup> Heleikonti batholith is exposed in the eastern limits of the study area. It occurs as an NW-SE elongated magmatic body composed of several interconnected plutons forming moderate to high relief. This complex intrudes the G. Heiani ophiolites to the north, Umm Radam metasediments to the east, and the Eqat ophiolitic mélangé to the west and south (Figs.1 & 3B). The plutons are mainly greyish-white, undeformed medium to coarse-grained felsic and foliated in parts, and enclose differently sized xenoliths of the relevant country rocks (Fig. 3C). Thermal metamorphism of the mélangé matrix is locally observed in the development of large, elongated, and randomly-oriented tourmaline porphyroblasts. The Hoteib pluton is 41 km<sup>2</sup>; a WNW-ESE elongated pluton occupies the northwestern part of the study area and is dissected by the Wadi Hoteib, where the Hoteib Ancient gold mine is located. It intrudes the ophiolites and metavolcanics of the Eqat shear zone (Fig. 3D). The rocks are highly foliated and mylonitized in parts, with their concordant foliation to that of the metavolcanics. The Eqat pluton is the smallest intrusion, with an area of about 11 km<sup>2</sup> that is located in the central part of the study area. It forms an E-W slightly elongated body, "Gabal Eqat," a remarkable landmark with a rugged relief towering over the southern part of Wadi Allaqi. Granitic rocks are reddish, massive, undeformed, spheroidally weathered, exfoliated, and jointed. These granitoids intrude the ophiolitic mélangé/metavolcanics to the east (Fig. 3E) and the gneissose tonalite-diorite westwards, showing sharp intrusive contacts. Along the Eqat shear zone, proper mylonitic fabric with quartz and feldspar porphyroclasts (Fig. 3F). All rocks are traversed by differently sized structurally controlled quartz-carbonate-epidote veins (Fig. 3G). They are moderately to steeply dipping NW-SE, NE-SW, and less commonly E-W trending. These veins experienced ductile deformation exemplified by pygmatic, upright folding, inference pattern, and boudinage structure (Fig. 3H).

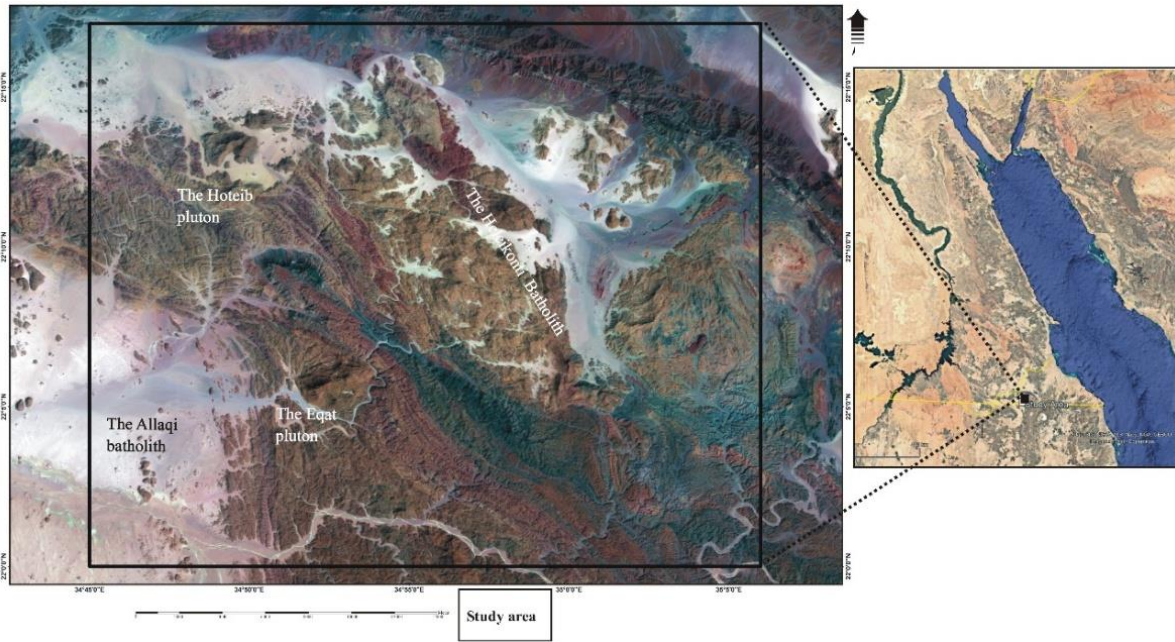


Fig. 1. A location map and a Landsat image showing the distribution of the magmatic rocks in the Eqat area, Southern Eastern Desert, Egypt.

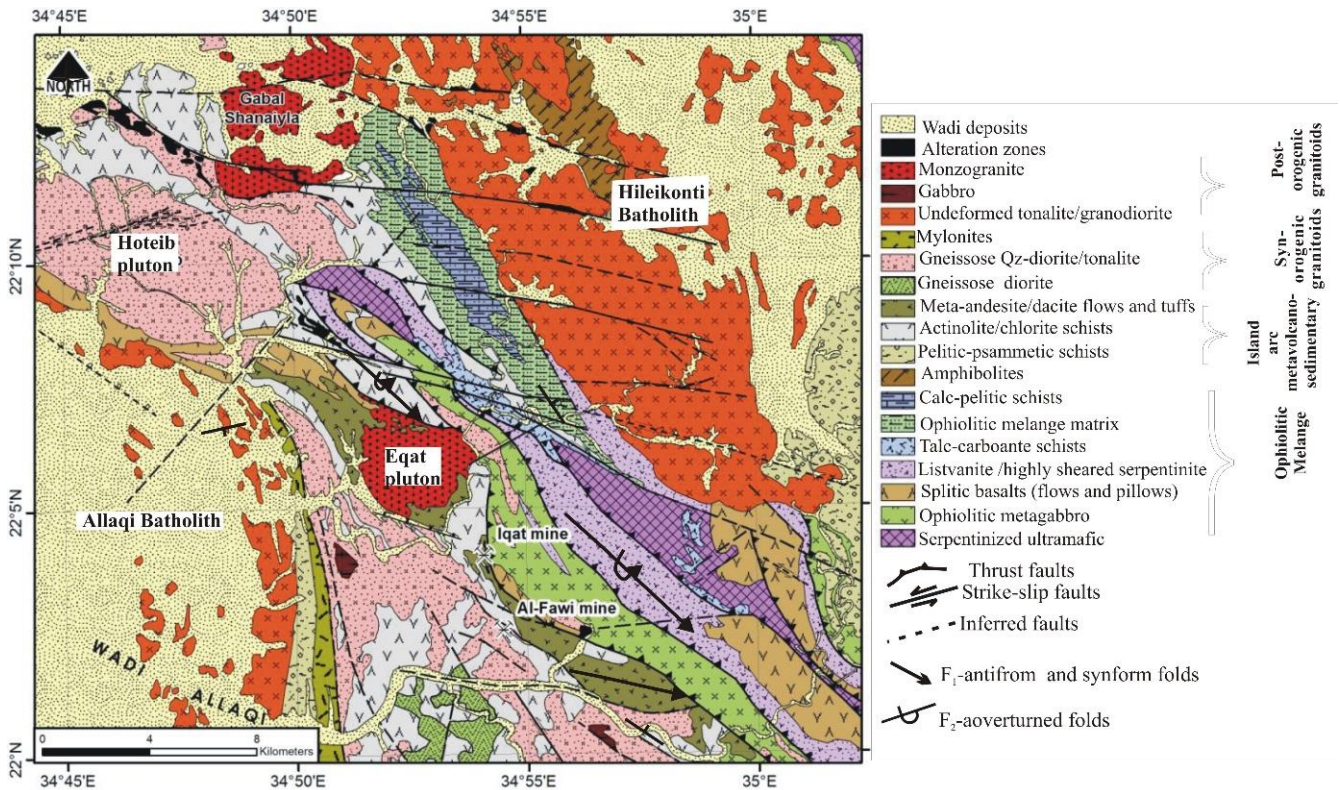
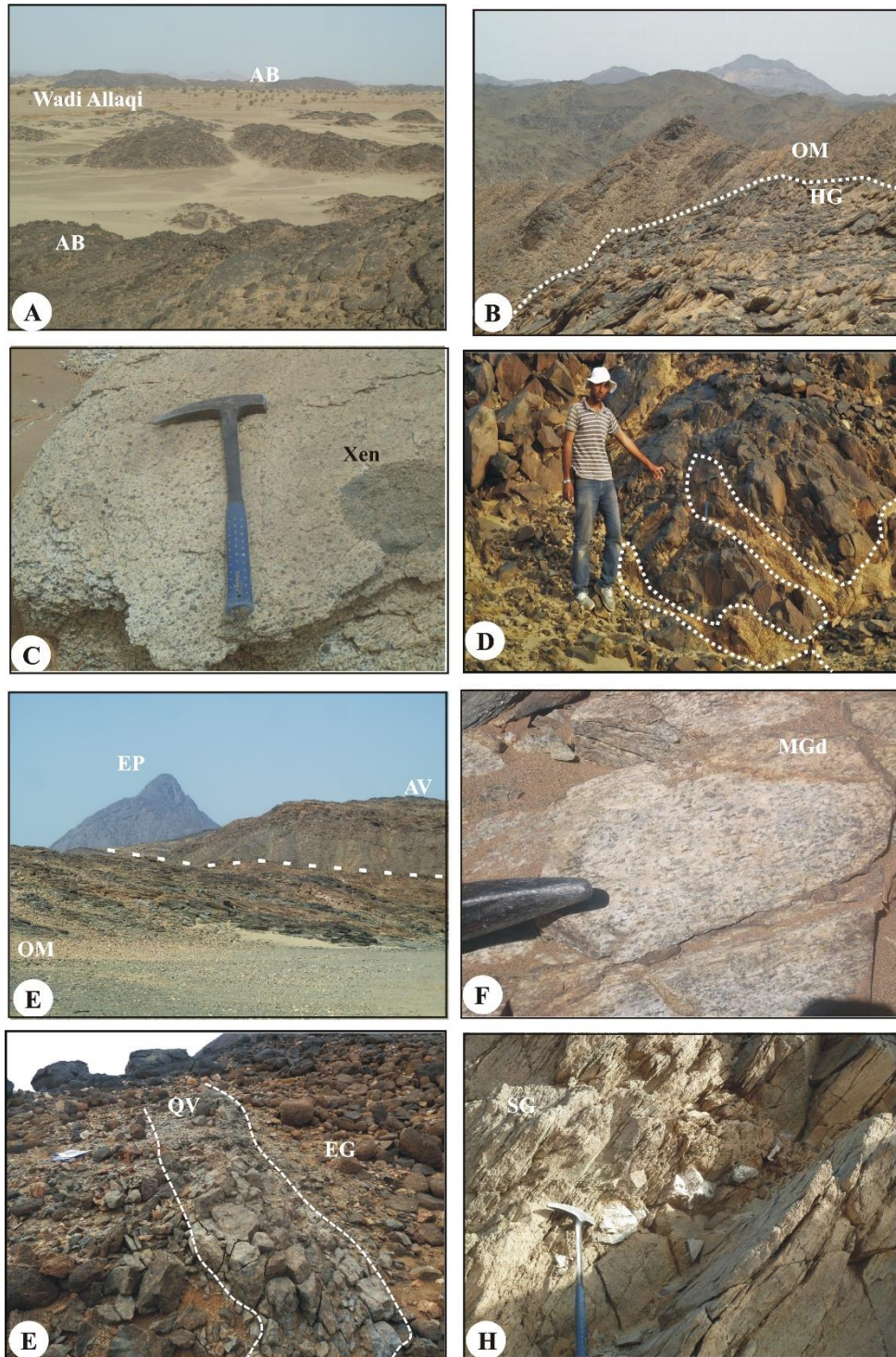


Fig. 2. A geologic map of the Eqat area (modified after Gabr et al., 2015 and Zohier and Emam, 2012).



**Fig. 3.** A) A general view of the composite Allaqi Batholith (AB), looking W., B) The locally foliated Heleikonti granitoid (HG) intruding the schistose ophiolitic mélangé (OM), looking NW., C) An elongated mafic xenolith (Xen) in a gneissose tonalite, Allaqi pluton., D) Off-shoots of the gneissose tonalite of the Hoteib Pluton in the island arc metavolcanics, looking W., E) The thrust contact between the ophiolitic mélangé (OM) and arc metavolcanics (AV), intruded by the Eqat pluton (EP), looking S., F) A mylonitized granodiorite (MGd) at the base of the Eqat pluton, with numerous quartz and feldspar porphyroclasts., G) A large folded highly sheared quartz vein (QV) invading the Eqat granite (EG), Wadi Eqat looking NW and H) A small boudinaged quartz vein in sheared granites (SG), Wadi Allaqi, looking S.

## Petrography

Petrographically, the studied rocks are felsic to intermediate in composition, ranging from syn-orogenic diorite, quartz diorite and tonalite, post-orogenic granodiorite, and monzogranite. The syn-orogenic rocks experience a pervasive gneissose fabric parallel to the foliations of the island arc assemblage. They comprise plagioclase (55-65%), Quartz (up to 30%), hornblende (4-10%), biotite (10-15%), and muscovite (up to 4%). The latter two minerals define the main foliation of the rocks; hornblende forms mineral lineation that is parallel to the main foliation (Fig. 4A). Quartz experiences different degrees of intracrystalline deformation exemplified by undulose extinction and deformational banding (Fig. 4B). Plagioclase ranges from andesine ( $An_{30-40}$ ) in the diorite/quartz diorite to frequently zoned oligoclase ( $An_{12-24}$ ) in the tonalite; crystals are often fractured and show selective alteration to sericite and or epidote (Fig. 4C). Zircon, apatite, magnetite, hematite, ilmenite, rutile, and minute gold grains are common accessory minerals. They also enclose mafic schlieren that is parallel to the foliation (Fig. 3A). The post-orogenic rocks are coarse to medium-grained, hypidiomorphic to panidiomorphic, and lack the presence of pervasive foliation, and are composed of quartz (30-35%), microcline (15-30%), and orthoclase (up to 12%) that are usually perthitized and plagioclase (15-30%) in the form of albite-oligoclase ( $An_{9-15}$ ). In the granodiorite, plagioclase and K-feldspars are of the same size (Fig. 4D). In the monzogranite, the larger tabular microcline often encloses smaller euhedral plagioclase crystals (Fig. 4E). Reddish-brown biotite (up to 10%), muscovite (5-8%), and less common green hornblende (up to 3%) show different modal proportions in both varieties. In addition to the accessory minerals recorded in the syn-orogenic rocks, pyrite, chalcopyrite, and marcasite are recorded. Both syn-orogenic and post-orogenic rocks experience mild to intense hydrothermal alteration associated with gold mineralization. These are exemplified by argillic (kaolinite), phyllic (illite), and propylitic of epidote, chlorite, and hematite. Depending on the adjacent country rock, the veins traversing the plutons are

either pure quartz or mixed with carbonate or epidote. For instance, near the serpentinites, quartz-carbonate veins are predominant and associated with listvenite (listwanite); near the island arc, metavolcanics and ophiolitic spilites, quartz-epidotes are more common. Textural criteria indicate that the syn-orogenic, post-orogenic varieties and the associated veins are sheared and mylonitized along the Eqat shear zone. Towards the shear zone, these rocks, including the Eqat pluton, range from sheared rocks to proper mylonites with bimodal size characteristics (Fig. 4F). All the minerals are affected by intracrystalline deformation, followed by recovery and dynamic recrystallization. These processes are demonstrated by wavy extinction, kink banding (Fig. 4G), and ribbon structure in quartz, kinking, and mineral fish in biotite (Fig. 4H), hornblende, and chlorite, and deformational twinning and mantled and fragmented porphyroclasts in feldspars. The mineral fish and mantled porphyroclasts (Fig. 4I) indicate a sinistral sense of shear to the Eqat shear zone. The presence of subgrains and curved to irregular grain boundaries of the quartz and feldspar neoblasts suggests that the dynamic recrystallization processes are of two types: subgrain rotation (SR) and low-temperature bulging (BLG) recrystallization at conditions of around 300-400 °C as reported by Passchier and Trouw (2005). This finding suggests that the Eqat shear zone developed under greenschist facies conditions.

## Geochemistry

Major oxides and trace elements of the studied rocks are presented (Tables 1 & 2). The chemical characteristics of the studied granitoids show that silica content shows a wide range (57.38- 78.35 wt%), alumina has a mild wide range (10.95- 16.1 wt%), and total alkalis range (3.4-9.4wt%). Depending on the indices used for granitic rocks classification (Frost et al., 2001), the modified alkali-lime ratio (MALI) from -6.4 to 7.5 indicates calcic to calc-alkalic granitoids. The alumina saturation index (ASI) ranges from 0.78 to 1.13, suggesting that most samples are meta-aluminous (ASI <1) except for six samples, which are peraluminous (ASI >1).

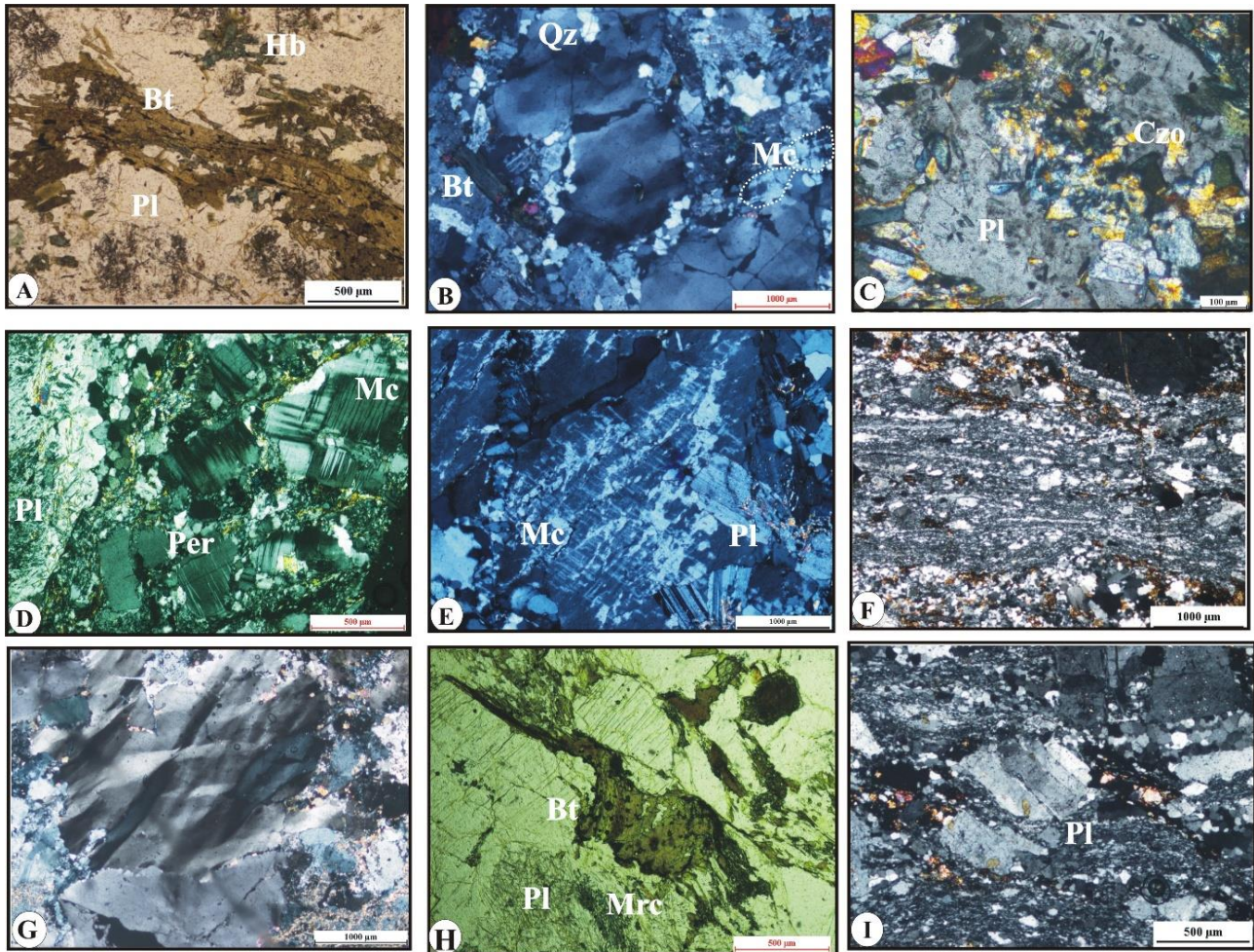


**Fig. 4.** A) A biotite (Bt) schlieren elongated in the direction of the main foliation of the rock; note the presence of small hornblende (Hb), gneissose diorite, PPL., B) Strained quartz (Qz) shows recrystallized grains along the boundaries. Note the presence of smaller biotite (Bt) flakes and microcline (Mc), CN., C) A large plagioclase crystal with clinzoisite crystals (Czo) in the core, gneissose tonalite, CN., D) A granodiorite showing two microcline (Mc) crystals with characteristic tartan twinning and a perthitized orthoclase (Per) crystal at the bottom of the photo, CN., E) A large tabular perthitized microcline (Mc) crystal encloses smaller plagioclase (Pl) prisms and is transacted by a quartz veinlet to the left, monzogranite, CN., F) A mylonitized monzogranite shows mylonitic foliation with larger strained feldspar and quartz in a recrystallized matrix, CN., G) Large quartz grains with conjugate kink bands. Note that the crystal's lower part is a subgrain separated from the kinked part by a thin veneer of recrystallized quartz, CN., H) A large biotite (Bt) mineral fish encloses dark radioactive haloes and indicates a sinistral sense of shear by its oblique orientation and stair-stepping, PPL. and I) A sigma-type mantled porphyroblast of plagioclase (Pl), stair-stepping to the left, shows a sinistral sense of shear, CN.

**Table 1. Major oxides (wt%) and some key ratios for the studied intrusive rocks of the study area.**

Lithology	Diorite				Tonalite								Granodiorite				Granite		
	S8-3	S15	S16	S7-1	S12	S19-1	S19-2	S24-2	S28	S37	S46-7	S48	S33-1	S46-3	S46-5	S30	S43-2	S47-6	S49-3
SiO <sub>2</sub>	63.14	63.74	63.56	64.87	69.35	57.38	67.16	67.02	72.87	61.68	71.74	68.03	74.62	78.35	75.08	63.32	76	76.49	76
TiO <sub>2</sub>	0.41	0.6	0.59	0.42	0.57	0.52	0.21	0.58	0.27	0.47	0.18	0.34	0.15	0.03	0.1	0.38	<0.01	0.35	0.2
Al <sub>2</sub> O <sub>3</sub>	15.82	15.51	15.37	15.13	12.93	14.81	14.16	12.87	12.6	16.1	14.15	15.32	13.41	11.52	12.82	11.1	12.87	10.95	11.53
Fe <sub>2</sub> O <sub>3t</sub>	4.19	5.1	4.94	4.26	4.79	9.23	4.83	5.67	3.95	3.43	2.89	3.28	1.49	1.68	2.8	5.51	0.86	2.48	3.22
MnO	<0.01	<0.01	<0.01	<0.01	<0.01	0.02	<0.01	0.01	<0.01	<0.01	<0.01	<0.01	<0.01	<0.01	0	0.01	0	<0.01	<0.01
MgO	3.02	3.5	3.64	3.09	1.28	4.92	1.1	1.59	0.94	1.88	0.42	1.65	0.18	<0.01	<0.01	1.12	<0.01	<0.01	<0.01
CaO	3.92	4.59	4.64	4.87	4.64	6.9	3.95	5.62	2.51	4.9	1.42	3.67	1.68	0.07	0.1	11.79	0.23	1.38	1.55
Na <sub>2</sub> O	4.45	3.77	3.99	4.25	4.58	3.22	3.8	3.72	5.15	4.87	4.19	4.48	3.69	3.42	3.53	5	5	5.57	5.28
K <sub>2</sub> O	0.85	1.4	1.38	0.99	0.01	0.19	0.5	0.35	0.32	1.64	3.56	1.42	3.59	4.11	4.77	0.36	4.36	0.22	0.76
P <sub>2</sub> O <sub>5</sub>	0.08	0.12	0.1	0.07	0.12	0.02	0.06	0.1	0.03	0.12	0.08	0.12	0.11	<0.01	0.02	0.06	<0.01	<0.01	<0.01
L.O.I.	3.8	1.33	1.44	1.73	1.43	2.46	3.9	2.15	1.01	4.59	1.04	1.37	0.77	0.58	0.63	1	0.35	2.31	1.18
Total	99.68	99.66	99.65	99.68	99.7	99.67	99.67	99.68	99.65	99.68	99.67	99.68	99.69	99.76	99.85	99.65	99.67	99.75	99.72
Na <sub>2</sub> O+K <sub>2</sub> O	5.3	5.17	5.37	5.24	4.59	3.41	4.3	4.07	5.47	6.51	7.75	5.9	7.28	7.53	8.3	5.36	9.36	5.79	6.04
MALI	1.38	0.58	0.73	0.37	-0.05	-3.49	0.35	-1.55	2.96	1.61	6.33	2.23	5.60	7.46	8.20	-6.43	9.13	4.41	4.49
ASI	1.04	0.97	0.94	0.90	0.82	0.82	1.02	0.78	0.94	0.87	1.07	0.99	1.04	1.13	1.15	0.37	0.96	0.92	0.94
F*No	0.56	0.57	0.55	0.55	0.77	0.63	0.80	0.76	0.79	0.62	0.86	0.64	0.88	1.00	1.00	0.82	0.99	1.00	1.00

MALE: Na<sub>2</sub>O+K<sub>2</sub>O-CaO  
 ASI: Al/Ca-1.67P+Na+K  
 F\*No: FeO\*/FeO\*+MgO

**Table 2. Trace and selected REE (ppm) of the studied intrusive rocks of the study area.**

Lithology	Diorite				Tonalite								Granodiorite				Granite		
	S8-3	S15	S16	S7-1	S12	S19-1	S19-2	S24-2	S28	S37	S46-7	S48	S33-1	S46-3	S46-5	S30	S43-2	S47-6	S49-3
V	74.9	76.6	98.9	103	49.7	206.6	49.8	83.3	43.6	70.9	33.9	52.8	25.1	12.2	21.7	122.8	9.4	120	9
Cr	84.7	57.9	54.7	58	33.9	73.4	27.2	23.4	16.2	120.2	83.8	181.4	17.6	77.4	148.8	160.4	60	157	59
Ni	27.1	20.9	19.5	20.5	11	18.7	5.8	9.7	9.2	8.5	13.1	11.8	6.2	10.5	13.4	41.7	11	42	12
Cu	8.7	16.8	48.3	18.4	<2	51.6	84.9	2.3	<2	16.6	15.5	13.4	4.6	3	3.8	62.7	<2	60	<2
Zn	42.2	43.5	50.8	54	18.8	76.3	29.1	33.9	21.5	39.1	40.9	38.8	19.3	86.7	101.4	17.9	60.4	18	62
Co	11.4	10.9	14	15.2	10.1	40.1	11.7	15.3	8.3	22	3.4	5	<2	<2	<2	16.2	<2	16	<2
Ga						19.7	14.9	19.7	15.1	19.9	23.8	19	17.3	30	28.7	13.9	34.2	14	34
Rb	20.4	15.8	24	23.3	<2	5.7	7.5	6.1	5.1	31.2	103.4	17.7	64	167.3	189.1	10	137.1	9	136
Sr	483.3	416.7	449.1	477.4	150.1	206.2	177	212.3	130.9	221.5	255.9	595.4	213.7	25.3	53.4	198	62.5	195	60
Zr	99.9	105.9	134.1	116.5	293.9	64	184.5	105.9	98.2	231	258.1	102.5	105.1	57.7	148.9	94.9	121.3	94	120
Nb	7.4	7.6	7.8	7.9	8.4	8.3	5.6	6.4	5.8	7.6	32	8.6	7.4	71.2	61.9	9.1	74.7	9	74
Ba	258.3	276.5	374.5	362.4	79.8	139	193	205.4	202.3	514.6	620.4	316	693.3	14	153.2	118.5	118.3	119	118
Ta	<2	<2	<2	<2	<2	2	<2	<2	<2	<2	<2	<2	<2	2	<2	<2	<2	<2	<2
Pb	3.8	5.3	6	4.8	4.6	10.9	2.5	4	4.6	4.4	27.1	5.4	16.3	17.6	19.7	3.9	57.3	3.8	56
Th	<2	<2	<2	<2	<2	<2	<2	<2	<2	5.6	15.5	14.6	5.4	20.5	24.2	<2	16.9	<2	16.9
La	<2	15.9	11.1	11.3	<2	<2	3	13.8	<2	12.2	56.1	<2	18	4.9	22.1	2.4	13.1	2.4	12.6
Y	<2	<2	<2	<2	6.8	11.2	<2	4.9	12.9	<2	34.2	<2	7.2	60.6	62.9	9.7	56.7	<2	<2
Yb	3	2.5	3.6	<2	<2	2.1	<2	<2	<2	<2	<2	<2	<2	3.2	3.8	5.8	<2	<2	<2

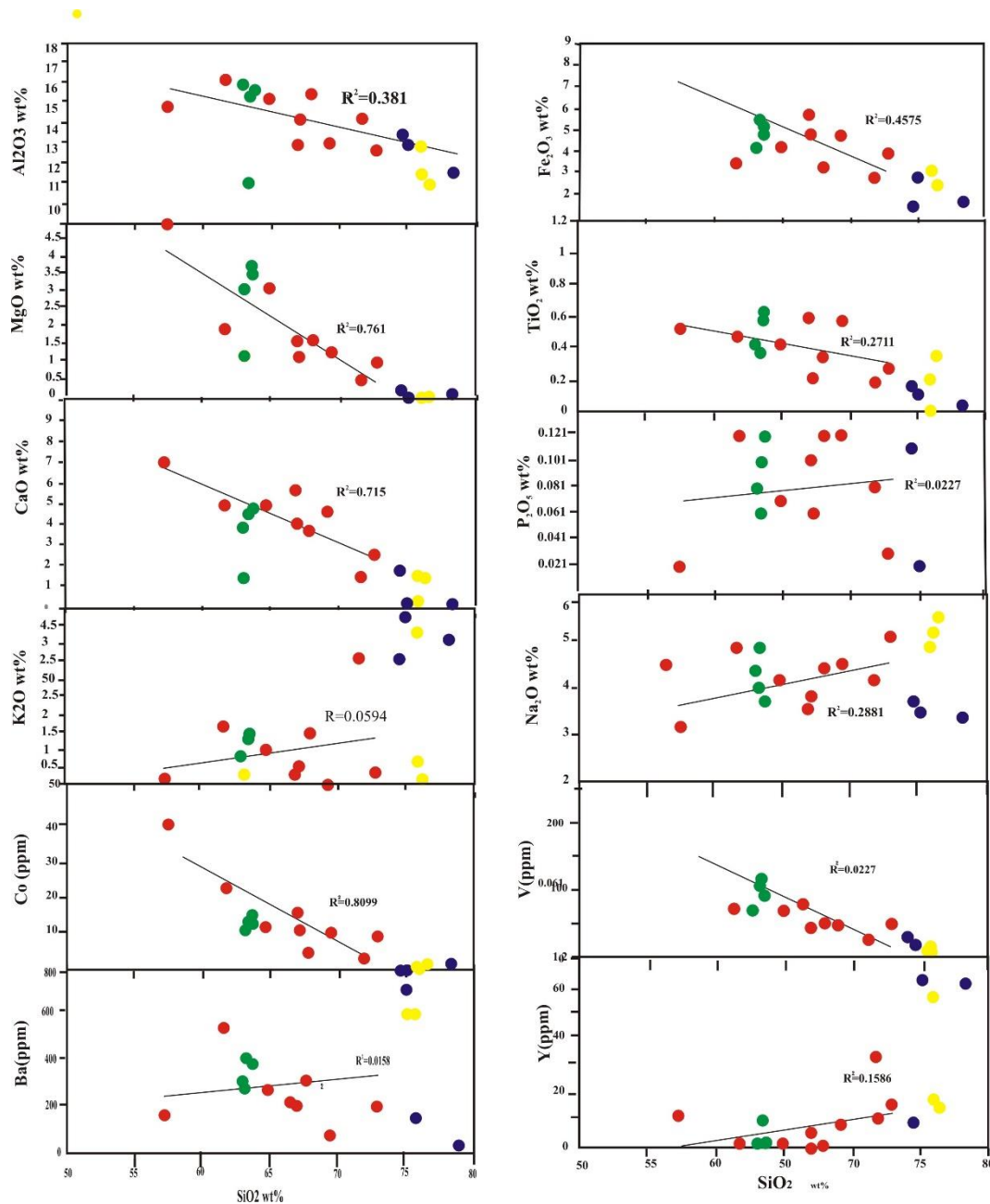


**Fig. 5. Harker variation diagrams for major oxides and selected trace elements for the Eqat granitoids Diorite/Qz-diorite Tonalite Granodiorite Granite.**

Depending on the Fe-number, the studied rocks belong to the magnesian to ferroan granitoids. This variation in indices might be attributed to the variation of the source or differentiation processes, as reported by Frost *et al.* (2001).  $\text{SiO}_2$ -based Harker variation diagrams for major oxides (Fig. 5) reveal that  $\text{TiO}_2$ ,  $\text{Al}_2\text{O}_3$ ,  $\text{Fe}_2\text{O}_3$ ,  $\text{MgO}$ , and  $\text{CaO}$  are inversely proportional to  $\text{SiO}_2$ , which reflects the effect of the fractionation of ferromagnesian minerals such as pyroxenes and amphiboles, plagioclase, titanomagnetite, sphene, and apatite during magma ascent.  $\text{K}_2\text{O}$  and  $\text{Na}_2\text{O}$  show a weak

positive correlation with silica. It is well known that a genetically related magmatic suite should have a good linear correlation between alkalis and silica (Wilson, 1989). The weak correlation in the Eqat suite might be attributed to different magma sources (mantle and crustal), crustal contamination, or interaction with post-magmatic hydrothermal fluids (Rollinson, 1993). As for the Harker variation diagrams for the trace elements, it is well documented that the compatible elements such as Co, V, and Zn are inversely proportional to the  $\text{SiO}_2$ , whereas the Ni, Cr, and Cu show more scatter

relation (Fig. 5). On the other hand, incompatible elements such as Ba, Rb, Sr, Zr, Th, and La with a positive correlation show much discrepancy than the major oxides (Fig. 5). It is well known that the behavior of trace elements in granitoids is more complex than major oxides for several reasons, including their incorporation in late-crystallized accessory minerals such as zircon, apatite, and sphene. In addition to crustal contamination, post-magmatic processes, and magma mixing are responsible for the deviation of the linear relation between elements, as seen in fractional crystallization processes (e.g., Fourcade and Allegre, 1981; Wilson, 1989; Spera et al., 2007). Chemically, the studied magmatic rocks are classified into quartz diorite, tonalite, granodiorite, and granite (Fig. 6A). Normalized spider diagrams are constructed to visualize and interpret the relative abundances of trace elements in a rock suite as a key indicator of its tectonic environment. The primitive mantle-normalized (McDonough and Sun, 1995) trace element diagram for the studied rocks shows the typical subduction-related magmatism pattern (Fig. 6B). It shows a negative spiked trend with an enrichment of the large ion lithophile elements (LILE), such as Rb, Ba, Th, and U, compared to the high field strength elements (HFSE), such as Zr, Hf, Nb, Ta and Ti. The curves show the depletion of some key elements that help to define the setting of the granitic rocks. Nb-Ta trough is a characteristic feature of arc-related magmatism, reflecting the retention of rutile in the subducted slab (Briqueu et al., 1984). The negative anomaly of P and Ti reflects the fractionation of apatite and iron oxides. Depletion of Y suggests the involvement of garnet fractionation in the source that gave rise to the granitic rocks. This depletion is common in arc-related I- and S-type granites (Chappell and White, 1974). The residual garnet is stable at a depth of 80 km, which means that the source of the studied granitic rocks is garnet lherzolite. The positive Pb anomaly suggests the influence of melt contamination by a crustal material. According to the Q-P diagram of Debon and Le Fort (1983), all the data follow the calc-alkaline trend of mantle-derived cefamic and mixed alumino-cefamic magmatic association with a characteristic pyroxene-amphibole-biotite mafic mineral assemblage (Fig. 6A). Based on the alumina saturation index of the A-B diagram (Villaseca et al., 1998), the studied rocks are mainly metaluminous, with few low to highly felsic peraluminous (Fig. 6C). Pearce et al. (1984)

utilized less mobile trace elements to differentiate the tectonic setting of granitoids. In the Rb versus Nb+Y binary diagram, most samples are situated within the volcanic arc granite field, apart from four samples that fall inside the plate granitoid field (Fig. 6D). Using the R1-R2 diagram (Batchelor and Bowden, 1985), the samples plot along the pre-plate collision, syn-orogenic to post-orogenic, a typical orogenic cycle that ends with alkaline granites (Fig. 6E). This systematic change reflects that the Eqat granitoid rocks formed first by pyroxene-plagioclase fractional crystallization of tholeiitic basaltic magma that gave rise to the intermediate rocks followed by episodic mixing with magma of crustal source that led to the formation of the more felsic and alkalic granites. To estimate the crustal thickness at the time of the granitic rocks' emplacement, we use the Rb-Sr diagram after Condie (1973). The studied rocks plot in the field of 20-30 km and, less commonly, 15-20 km, reflecting the crust thickening process during the emplacement of the different granitic rocks (Fig. 6F). The 20-30 km thickness is typical for calc-alkaline series in an island arc setting, such as in the present Viti Levu arc in the Fiji island arc complex (e.g., Chen et al., 2019; Gill et al., 2022). This intermediate crustal thickness corresponds to an intermediate subduction depth of 100-200km (Condie et al., 1972). Generally, the Pan-African granitic magmatism in the Eastern Desert and Sinai belongs to two phases: the 750–610 Ma island arc older syn-to-late-orogenic granites and the 610-530 Ma younger post-orogenic to anorogenic granites (El-Bialy, 2020, and references therein). Field, petrographic, and geochemical criteria indicate that the syn-orogenic, deformed diorite-tonalite of the Hoteib pluton and the Allaqi batholith belong to the older island arc phase. These rocks may originate from a mantle mafic source subjected to fractional crystallization followed by assimilation with crustal material (e.g., Eliwa et al., 2014) or from a high degree of fractional crystallization of crustal mafic melts generated from a lower crust amphibolite source (e.g., Farahat et al., 2007). Our data from the diagram of Batchelor and Bowden (1985) indicate that mixing between mantle source and crustal assimilation is consistent with the first opinion. On the other hand, the younger granite phase is classified chemically into a 610-580Ma undeformed calc-alkaline, meta-aluminous to slightly peraluminous I-type phase and a 580-530Ma alkaline-peralkaline, peraluminous A-type phase (Fowler and Hamimi 2020).

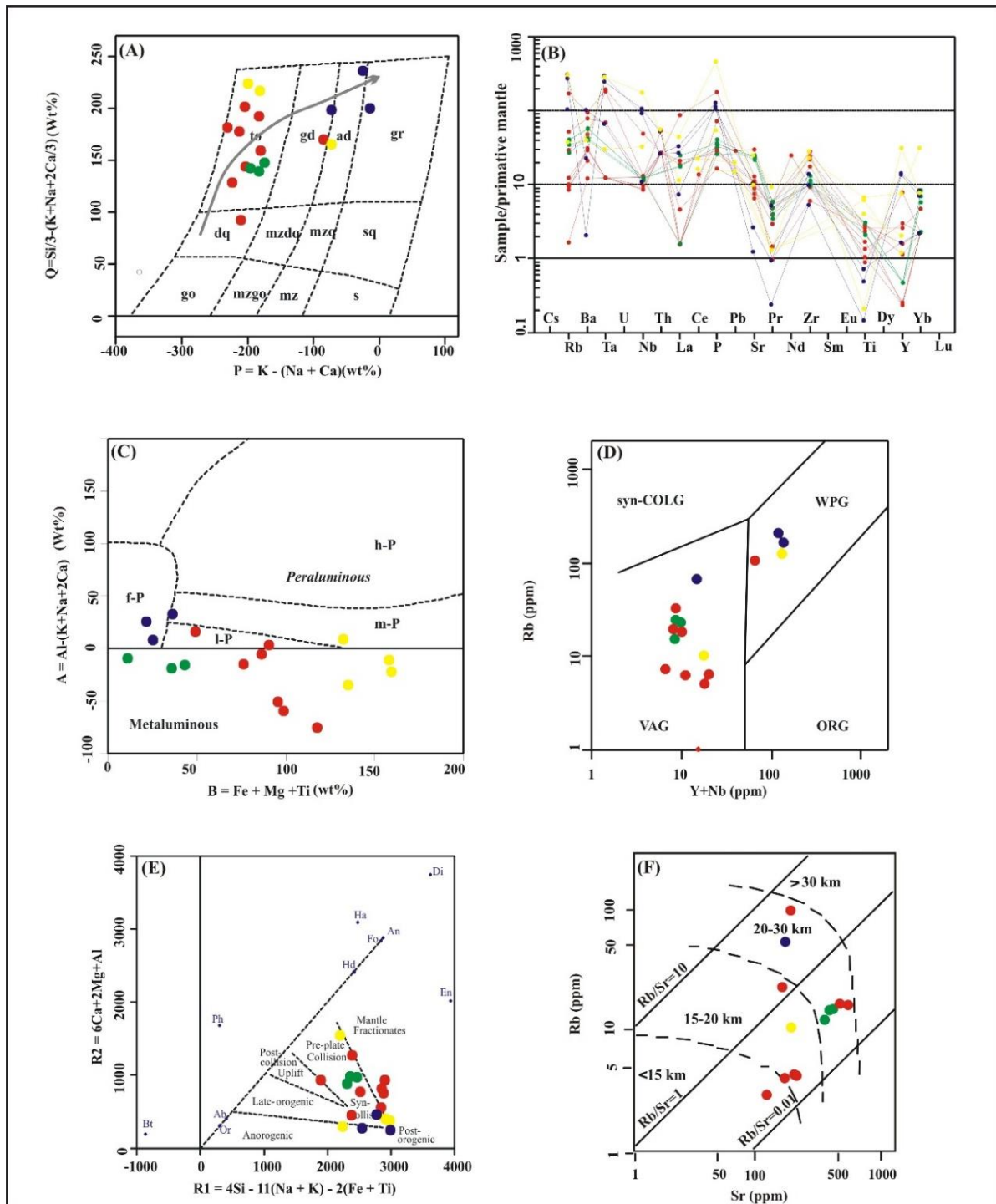


Fig. 6. A) P-Q Debon and Le Fort (1983), the grey line represents the calc-alkaline trend of the cefamic and aluminocefamic association to: tonalite, dq: quartz diorite, go: gabbro, mzgo: monzogabbro, mzdq: quartz monzodiorite, gd: granodiorite, mz: monzonite, mzq: quartz monzonite, ad: adamellite, s: syenite, sq: quartz syenite, gr: granite. B) A primitive mantle-normalized spider diagram for trace elements normalizing values adopted from (McDonough and Sun, 1995). C) B-A Plot (modified by Villaseca *et al.*, 1998), (lp) low peraluminous granitoids, (mp) moderately peraluminous granitoids, (hp) highly peraluminous granitoids, (fp) highly felsic peraluminous granites D) Rb vs (Y+Nb) discrimination diagram for the studied granites (after Pearce *et al.*, 1984), that shows the fields of Syn-COLG: syn-collisional granites, WPG: within-plate granites, VAG: volcanic-arc granites and ORG: ocean-ridge granites. E) R1-R2 binary diagram for granitic rocks (Batechelor and Bowden, 1985). F) Rb-Sr diagram that shows crustal thickness for the studied granitic intrusions as inferred from the crustal thickness index (Condie, 1973).

The Heleikonti batholith and the Eqat pluton belong to the 610–580 Ma I-type younger post-collisional phase. The lack of A-type granite in the Eqat area may be attributed to one or several reasons (Frost et al., 2001). The source of these rocks should be dry and have a high temperature (Whalen et al., 1987; King et al., 1997), which is unlikely to be the situation of the Eqat area, as such subduction environment is of lower temperature and enriched in fluid contents, promoting I- and S-type granites emplacement.

### Conclusions

Field and petrographic studies of the Eqat intrusive rocks assigned two types of granitoids: syn-orogenic gneissose greyish white rocks of dioritic to tonalitic composition that are composed mainly of plagioclase+ hornblende+ biotite+ muscovite± quartz with a pervasive foliated fabric. A post-orogenic greyish white tonalitic granodioritic to reddish monzogranitic elongated bodies with a composition of quartz + K-feldspar+ plagioclase+ biotite+ muscovite ±hornblnde. Near the Eqat shear zone, both groups are locally mylonitized, with several shear sense indicators from outcrop and microscopical scales, demonstrating the sinistral strike-slip shear for the Eqat shear zone. Geochemical signatures indicate these rocks are calc-alkaline, meta-aluminous to slightly peraluminous, and ferroan to magnesian granitoids. This pre-plate collision, syn-orogenic to post-orogenic evolution, is a typical orogenic cycle that ends with alkaline granites. They were emplaced on an island arc setting with a thickness (20-30 km), similar to the present Viti Levu island arc.

### Acknowledgements

The authors are grateful to the Egyptian Mineral Resources Authority (EMRA) for facilitating the fieldwork, preparation of thin sections, and geochemical analyses, which were carried out at the Central Laboratories of EMRA at Dokki.

### References

- Akaad MK, Noweir AM (1980). Geology and lithostratigraphy of the Arabian Desert orogenic belt of Egypt between latitudes 25°35' and 26°35'N. In: Cooray PG, Tahoun SA (eds) Evolution and mineralization of the Arabian-Nubian Shield. Inst. Appl. Geol. Jeddah Bull., Pergamon, Oxford, 3, 127–135.
- Azer MK (2013). Late Ediacaran (605–580 Ma) post-collisional alkaline magmatism in the Arabian-Nubian Shield: a case study of Serbal ring-shaped intrusion, southern Sinai, Egypt. *J Asia Earth Sci* 77:203–223.
- Basta FF, Maurice AE, Bakhit BR, Azer MK, El-Sobky AF (2017). Intrusive rocks of the Wadi Hamad Area, North Eastern Desert, Egypt: change of magma composition with maturity of Neoproterozoic continental island arc and the role of collisional plutonism in the differentiation of arc crust. *Lithos* 288–289:248–263.
- Batchelor RA, Bowden P (1985). Petrogenetic Interpretation of Granitoid Rock Series Using Multicationic Parameters. *Chemic. Geol.*, 48, 43–55.
- Bentor YK (1985). The crustal evolution of the Arabo-Nubian Massif with special reference to the Sinai Peninsula. *Precambr Res* 28:1–74.
- Briqueu L, Bougault H, Joron JL (1984). Quantification of Nb, Ta, Ti and V anomalies in magmas associated with subduction zones: Petrogenetic implications. *Earth Planet Sci Lett*, 68, 2, 297–308.
- Chappell BW, White AJ R, (1974). Two contrasting granite types. *Geology*, 2,10,569–574.
- Chen J, Chen YJ, Wiens DA, Weid SS, Zha Y, Julia J, Cai C (2019). Crustal and lithospheric structure of inactive volcanic arc terrains in Fiji. *Tectonophysics* 750, 394–403.
- Condie KC (1973). Archean Magmatism and Crustal Thickening. *GSA Bulletin*, 84, 9, 2981–2992.
- Condie KC, Swenson DH, Hayslip DL (1972). Geochemical indices of crustal thickness and depth to Benioff zone: *Geol. Soc. America Abs. with Programs (Cordilleran Sec.)*, 4, 3, 138–139.
- Debon F, Le Fort P (1983). A chemical-mineralogical classification of common plutonic rocks and associations. *Transactions of the Royal Society of Edinburgh: Earth Sci.*, 73, 135–149.
- El-Bialy MZ, Hassen IS (2012). The late Ediacaran (580–590 Ma) onset of anorogenic alkaline magmatism in the Arabian-Nubian Shield: Katherina A-type rhyolites of Gabal Ma'ain, Sinai, Egypt. *Precambr Res* 216–219, 1–22.
- El-Bialy, MZ (2020): Precambrian basement complex of Egypt. In Hamimi Z, El-Barkooky A, Martínez Frías J, Fritz H, Abd El-Rahman Y (eds) *The geology of Egypt. Regional geology reviews*. Springer Nature Switzerland, 38–80. [https://doi.org/ 10.1007/978-3-030-15265-9\\_2](https://doi.org/10.1007/978-3-030-15265-9_2)
- El Gaby S, El Nady O, Khudeir A (1984). Tectonic evolution of the basement complex in the Central Eastern Desert of Egypt. *Geol. Rundsch.*, 73, 1019–1036.
- El Ramly MF (1972). A new geological map for the basement rocks in the Eastern and Southwestern Deserts of Egypt. *Ann. Geol. Surv. Egypt*, 2, 1–18.
- El Shazly EM (1964). On the classification of the Precambrian and other rocks of magmatic affiliation in Egypt, U. A. R. In: *Proceedings of 24th International Geological Congress, India*, 5, 88–101.
- Eliwa HA et al. (2014). SIMS zircon U-Pb and mica K–Ar geochronology, and Sr–Nd isotope geochemistry of Neoproterozoic granitoids and their bearing on the evolution of the north Eastern Desert, Egypt. *Gondwana Res.*, 25, 1570–1598.
- Farahat ES, Mohamed HA, Ahmed AF, El Mahallawi MM (2007). Origin of I- and A-type granitoids from the

- Eastern Desert of Egypt: implications for crustal growth in the northern Arabian-Nubian Shield. *J. Afr. Earth Sci.*, 49, 43–58.
- Fourcade S, Allegre CJ (1981). Trace Elements Behavior in Granite Genesis: A case study of the calc-alkaline plutonic association from the Querigut complex (Pyrenees, France). *Contrib. Mineral. Petrol.*, 76, 177, 1-95.
- Fowler, A., Hamimi, Z., (2020): Structural and tectonic framework of the Neoproterozoic basement of Egypt: from gneiss domes to transpression Belts. In Hamimi Z, El-BarkookyA, Martínez Frías J, Fritz H, Abd El Rahman Y (eds) *The geology of Egypt. Regional geology reviews*. Springer Nature Switzerland, 81–129. [https://doi.org/10.1007/978-3-030-15265-9\\_2](https://doi.org/10.1007/978-3-030-15265-9_2).
- Frost BR, Calvin GB, William JC, Richard JA, David JE, Carol DF (2001). A geochemical classification for granitic rocks. *J. Petrol.*, 42, 11, 2033-2048.
- Gabr, S.S., Hassan, S.M., Sadek, M.F., (2015). Prospecting for new gold-bearing alteration zones at El-Hoteib area, south Eastern Desert, Egypt, using remote sensing data analysis. *Ore Geol. Rev.*, 71, 1-13.
- Gill J, Todd E, Hoernle K, Hauff F, Ann Price A, Jackson MG (2022). Breaking up is hard to do: magmatism during oceanic arc breakup, subduction reversal, and cessation. *Geochemistry, Geophysics, Geosystems*, 23, e2022GC010663. <https://doi.org/10.1029/2022GC010663>.
- Greiling RO, de Wall H, Sadek MF, Dietl C (2014). Late Pan-African granite emplacement during regional deformation, evidence from magnetic fabric and structural studies in the Hammamat–Atalla area, Central Eastern Desert of Egypt *J. Afric. Earth Sci.*, 99, 109–121.
- Hassan MA, Hashad AH (1990). Precambrian of Egypt. In: Said R (ed) *The geology of Egypt*. Balkema, Rotterdam, 201–248.
- Hussein, A.A., Ali, M.M., and El Ramly, M.F., (1982): A proposed new classification of the granites of Egypt. *J. Volc. Geoth. Res.*, 14, 187-198.
- King, P. L., White, A. J. R., Chappell, B. W., & Allen, C. M. (1997). Characterization and origin of aluminous A-type granites from the Lachlan Fold Belt, southeastern Australia. *J. Petrol.*, 38, 3, 371–39.
- Klemm R, Klemm D (2013). Gold and gold mining in Ancient Egypt and Nubia, geoarchaeology of the Ancient gold mining sites in the Egyptian and Sudanese Eastern Deserts. Springer-Verlag, Berlin, Heidelberg, 663p.
- McDonough WF, Sun SS (1995). The composition of the Earth. *Chem. Geol.*, 120, 3-4, 223-253.
- Moghazi AM, Hassanen MA, Mohamed FH, Ali S (2004). Late Neoproterozoic strongly peraluminous leucogranites, Southern Eastern Desert, Egypt: petrogenesis and geodynamic significance. *Miner. Petrol.*, 81, 19-41.
- Moussa EMM, Stern RJ, Manton WI, Ali KA (2008). SHRIMP zircon dating and Sm/Nd isotopic investigations of Neoproterozoic granitoids, Eastern Desert, Egypt. *Precamb. Res.* 160, 341–356.
- Nasr, B.B., Masoud, M.S., El, Sherbeni, H., Makhlof, A.A., (1998): Some new occurrences of gold mineralization, Eastern Desert, Egypt. *Ann. of the Geol. Survey of Egypt* 21, 331–344.
- Oweiss, Kh.A., and Said, M.M., (2000): Geological and geochemical exploration for gold at Um Egat (Al Fawi) area, south Eastern Desert, Egypt. *Ann. of the Geol. Survey of Egypt* 23(2), 609–613.
- Passchier, CW., and Trouw RAJ (2005). *Microtectonics*, 2<sup>nd</sup> edition. Springer-Verlag Berlin Heidelberg, 336p.
- Pearce JA, Harris NBW, Tindle AG (1984). Trace element discrimination diagram for the tectonic interpretation of granitic rocks. *J. Petrol.*, 25, 4, 956-983.
- Ries AC, Shackelton RM, Graham RH, Fitches, WR (1983). Pan-African structures, ophiolites and mélange in the Eastern Desert of Egypt: a traverse at 26°N. *J. Geol. Soc. London* 140,75–95.
- Rollinson H (1993). *Using geochemical data: evaluation, presentation, interpretation*. John Wiley and Sons Inc., New York, 350p.
- Salem SM (2007). Using remote sensing techniques in the geology and gold mineralization at Al Faw Eqat area, South Eastern Desert, Egypt. *Egypt. J. Remote Sens. Space Sci.*, 10, 137–150.
- Spera FG, Bohrsen WA, Till CB, Ghorso MS (2007). Partitioning of trace elements among coexisting crystals, melt, and supercritical fluid during isobaric crystallization and melting. *Amer. Min.*, 92, 1881-1898.
- Villaseca C, Barbero L, Rogers G (1998). Crustal origin of Hercynian peraluminous granitic batholiths of central Spain: petrological, geochemical and isotopic (Sr, Nd) arguments. *Lithos*, 43, 55-79.
- Whalen, J. B., Currie, K. L., Chappell, B. W., & England, R. N. (1987). A-type granites: geochemical characteristics, discrimination, and petrogenesis. *Contrib. Mineral. Petrol.*, 95, 407–419.
- Wilson M (1989). *Igneous petrogenesis, a global tectonic approach*. Springer, The Netherlands. 480p.
- Zoheir B, Emam A (2012). Integrating geologic and satellite imagery data for high-resolution mapping and gold exploration targets in the South Eastern Desert, Egypt. *J. Afric. Earth Sci.*, 66-67, 22-34.

## أصل الصخور الجرانيتية بجبل إيقات، جنوب الصحراء الشرقية، مصر

نهلة أحمد شلالى<sup>١</sup>، ومحمود السيد المزين<sup>٢</sup>، ومجد عبد الحميد الشرقاوي<sup>١</sup>، ومجد السباعي<sup>٢</sup>، وأشرف العزب<sup>٣</sup>

<sup>١</sup> قسم الجيولوجيا، كلية العلوم، جامعة القاهرة، الجيزة، مصر

<sup>٢</sup> الهيئة المصرية العامة للثروة المعدنية، القاهرة، مصر

<sup>٣</sup> هيئة المواد النووية، القطامية، القاهرة، مصر

تتكوّن منطقة إيقات من حزام دفع وطي يتألف من مزيج أوفيو ليتي وتجميع بركاني متحول لقوس جُزر، وقد تخلل هذه المنطقة أربع كتل نارية. وتشمل هذه الكتل باثوليثي العلاقي وهيليكونتي، اللذان يتكونان من عدة بلوتونات مدمجة ذات تركيب متوسط إلى فلسي. أما بلوتونا حوتيب وإيقات، فيقعان في شمال المنطقة ووسطها، ويتكوّنان بشكل رئيسي من صخور فلسية. تشير العلاقات الحقلية والمعايير النسيجية إلى أن صخور العلاقي وحوتيب تنتمي إلى الجرانيتويدات المترامنة مع الطور الأوروجيني، والتي تتميز بنسيج نيسي مواز لتورق صخور تجميع أقواس الجُزر/المزيج الأوفيو ليتي. بينما تنتمي صخور هيليكونتي وإيقات إلى الجرانيتويدات التي تلت الطور الأوروجيني، وتُظهر نسيجاً نارياً غير مشوّه. من الناحية البتروجرافية، تتكون من صخور الديوريت، التوناليت، الجرانديوريت، والمونزوجرانيت، بنسب متفاوتة من الكوارتز والبلاجيوكليز وفلسبارات البوتاسيوم والميكا والهورنبلند. وتشير المعايير النسيجية إلى أن كلا المجموعتين تأثرتا بالتفكك المحلي (الميلونيتة) على طول منطقة القص في إيقات، أي أن هذه المنطقة القصية نشأت بعد العمليات النارية. وأثبتت الدراسة الجيوكيميائية أن هذه الصخور تنتمي إلى النوع I، كالس-قلوية إلى قلوبية، جرانيتويدات قوس بركاني إلى داخل اللوح والتي قد تم توطينها ضمن قشرة أرضية يتراوح سمكها بين ٢٠ و ٣٠ كيلومتراً.